Observation of Berry's Phase in a Solid State Qubit

P. J. Leek,[1] J. M. Fink,[1] A. Blais,[2] R. Bianchetti,[1] M. Göppl,[1] J. M. Gambetta,[3,4]
D. I. Schuster,[4] L. Frunzio,[4] R. J. Schoelkopf,[4] and A. Wallraff[1]

[1]*Department of Physics, ETH Zürich, CH-8093, Zürich, Switzerland.*
[2]*Département de Physique, Université de Sherbrooke, Sherbrooke, Québec, J1K 2R1 Canada.*
[3]*Institute for Quantum Computing and Department of Physics and Astronomy,*
University of Waterloo, Waterloo, Ontario, N2L 3G1 Canada.
[4]*Departments of Applied Physics and Physics, Yale University, New Haven, CT 06520, USA.*
(Dated: November 1, 2007)

In quantum information science, the phase of a wavefunction plays an important role in encoding information. While most experiments in this field rely on dynamic effects to manipulate this information, an alternative approach is to use geometric phase, which has been argued to have potential fault tolerance. We demonstrate the controlled accumulation of a geometric phase, Berry's phase, in a superconducting qubit, manipulating the qubit geometrically using microwave radiation, and observing the accumulated phase in an interference experiment. We find excellent agreement with Berry's predictions, and also observe a geometry dependent contribution to dephasing.

When a quantum mechanical system evolves cyclically in time such that it returns to its initial physical state, its wavefunction can acquire a geometric phase factor in addition to the familiar dynamic phase [1, 2]. If the cyclic change of the system is adiabatic, this additional factor is known as Berry's phase [3], and is, in contrast to dynamic phase, independent of energy and time.

In quantum information science [4], a prime goal is to utilize coherent control of quantum systems to process information, accessing a regime of computation unavailable in classical systems. Quantum logic gates based on geometric phases have been demonstrated in both nuclear magnetic resonance [5] and ion trap based quantum information architectures [6]. Superconducting circuits [7, 8] are a promising solid state platform for quantum information processing [9–14], in particular due to their potential scalability. Proposals for observation of geometric phase in superconducting circuits [15–19] have existed since shortly after the first coherent quantum effects were demonstrated in these systems [20].

Geometric phases are closely linked to the classical concept of parallel transport of a vector on a curved surface. Consider, for example, a tangent vector v on the surface of a sphere being transported from the North pole around the path P shown in Fig. 1A, with v pointing South at all times. The final state of the vector v_f is rotated with respect to its initial state v_i by an angle ϕ equal to the solid angle subtended by the path P at the origin. Thus, this angle is dependent on the geometry of the path P, and is independent of the rate at which it is traversed. As a result, departures from the original path that leave the solid angle unchanged will not modify ϕ. This robustness has been interpreted as a potential fault tolerance when applied to quantum information processing [5].

The analogy of the quantum geometric phase with the above classical picture is particularly clear in the case of a two-level system (a qubit) in the presence of a bias field that changes in time. A familiar example is a spin-

1/2 particle in a changing magnetic field. The general Hamiltonian for such a system is $H = \hbar R \cdot \sigma/2$, where $\sigma = (\sigma_x, \sigma_y, \sigma_z)$ are the Pauli operators, and R is the bias field vector, expressed in units of angular frequency. The qubit dynamics is best visualized in the Bloch sphere picture, in which the qubit state s continually precesses about the vector R, acquiring dynamic phase $\delta(t)$ at a rate $R = |R|$ (see Fig. 1B). When the direction of R is now changed adiabatically in time (i.e. at a rate slower than R), the qubit additionally acquires Berry's phase, while remaining in the same superposition of eigenstates with respect to the quantization axis R. The path followed by R in the three dimensional parameter space of
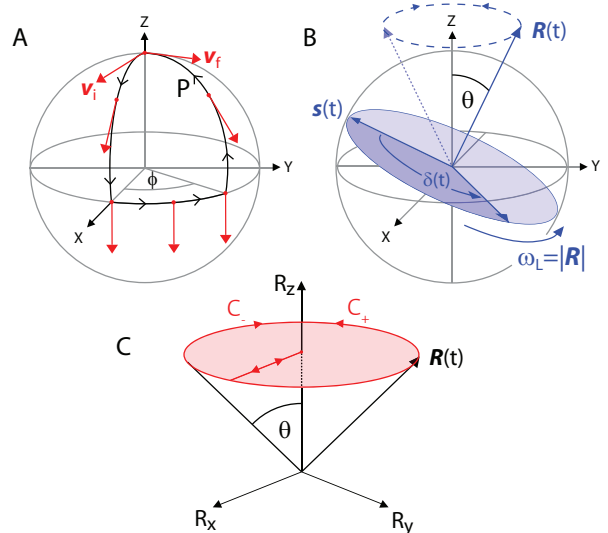

FIG. 1: (**A**) Parallel transport of the vector v_i on a spherical surface around the closed path P results in it rotating by a geometric angle ϕ to v_f when it returns to its initial position. (**B**) Dynamics of the Bloch vector s of a qubit in the presence of a bias field R tilted by an angle θ from the z-axis. (**C**) Parameter space of the Hamiltonian for the same case.

the Hamiltonian (see Fig. 1C) is the analogue of a path in real space in the classical case. When $\boldsymbol{R}$ completes the closed circular path C, the geometric phase acquired by an eigenstate is $\pm\Theta_C/2$ [3], where Θ_C is the solid angle of the cone subtended by C at the origin. The $\pm$ sign refers to the opposite phases acquired by the ground or excited state of the qubit, respectively. For the circular path shown in Fig. 1C, the solid angle is given by $\Theta_C = 2\pi(1 - \cos\theta)$, depending only on the cone angle θ.

We describe an experiment carried out on an individual two-level system realized in a superconducting electronic circuit. The qubit is a Cooper pair box [21, 22] with an energy level separation of $\hbar\omega_{\mathrm{a}} \approx h \times 3.7$ GHz when biased at charge degeneracy, where it is optimally protected from charge noise [23]. The qubit is embedded in a one-dimensional microwave transmission line resonator with resonance frequency $\omega_{\mathrm{r}}/2\pi \approx 5.4$ GHz (see Fig. 2A). In this architecture, known as circuit quantum electrodynamics (QED) [24, 25], the qubit is isolated effectively from its electromagnetic environment, leading to a long energy relaxation time of $T_1 \approx 10$ μs, and a spin-echo phase coherence time of $T_2^{\mathrm{echo}} \approx 2$ μs. In addition, the architecture allows for a high visibility dispersive readout of the qubit state [26].

Fast and accurate control of the bias field $\boldsymbol{R}$ for this superconducting qubit is achieved through phase and amplitude modulation of microwave radiation coupled to the qubit through the input port of the resonator (see Fig. 2A). The qubit Hamiltonian in the presence of such radiation is

$$H = \frac{\hbar}{2}\omega_{\mathrm{a}}\sigma_z + \hbar\Omega_{\mathrm{R}}\cos(\omega_{\mathrm{b}}t + \varphi_R)\sigma_{\mathrm{x}},$$

where $\hbar\Omega_{\mathrm{R}}$ is the dipole interaction strength between the qubit and a microwave field of frequency ω_{b} and phase φ_R. Thus $\Omega_{\mathrm{R}}/2\pi$ is the Rabi frequency that results from resonant driving. The above Hamiltonian may be transformed to a frame rotating at the frequency ω_{b} using the unitary transformation $H' = UHU^{-1} - i\hbar U\dot{U}^{-1}$, where $U = e^{i\omega_b t\sigma_z/2}$. Ignoring terms oscillating at $2\omega_b$ (the rotating wave approximation), the transformed Hamiltonian takes the form

$$H' \approx \frac{\hbar}{2}(\Delta\sigma_z + \Omega_x\sigma_x + \Omega_y\sigma_y),$$

where $\Omega_x = \Omega_{\mathrm{R}}\cos\varphi_R$ and $\Omega_y = \Omega_{\mathrm{R}}\sin\varphi_R$. This is equivalent to the generic situation depicted in Fig. 1B and C, with $\boldsymbol{R} = (\Omega_x, \Omega_y, \Delta)$ and $\Delta = \omega_{\mathrm{a}} - \omega_{\mathrm{b}}$ being the detuning between the qubit transition frequency and the applied microwave frequency. In our experiment we keep Δ fixed, and control the bias field to trace circular paths of different radius Ω_{R}.

We measure Berry's phase in a Ramsey fringe interference experiment by initially preparing an equal superposition of the qubit ground and excited states, which acquires a relative geometric phase $\gamma_C = 2\pi(1 - \cos\theta)$,

equal to the total solid angle enclosed by the cone depicted in Fig. 1C, with $\cos\theta = \Delta/(\Omega_{\mathrm{R}}^2 + \Delta^2)^{1/2}$. As the bias field adiabatically follows the closed path $C_{\pm}$, the qubit state acquires both a dynamic phase $\delta(t)$ and a geometric phase γ_C, corresponding to a total accumulated phase $\phi = \delta(t) \pm \gamma_C$ (the $\pm$ sign denoting path direction) which we extract by performing full qubit state tomography [4]. To directly observe only the geometric contribution, we use a spin echo [27] pulse sequence that cancels the dynamic phase as explained below.

The complete sequence (see Fig. 2B) starts by preparing the initial σ_z superposition state with a resonant $\pi/2$ pulse. Then the path C_- is traversed, causing the qubit to acquire a phase $\phi_- = \delta(t) - \gamma_C$. Applying a resonant spin echo π pulse to the qubit about an orthogonal axis now inverts the qubit state, effectively inverting the phase ϕ_-. Traversing the control field path again, but
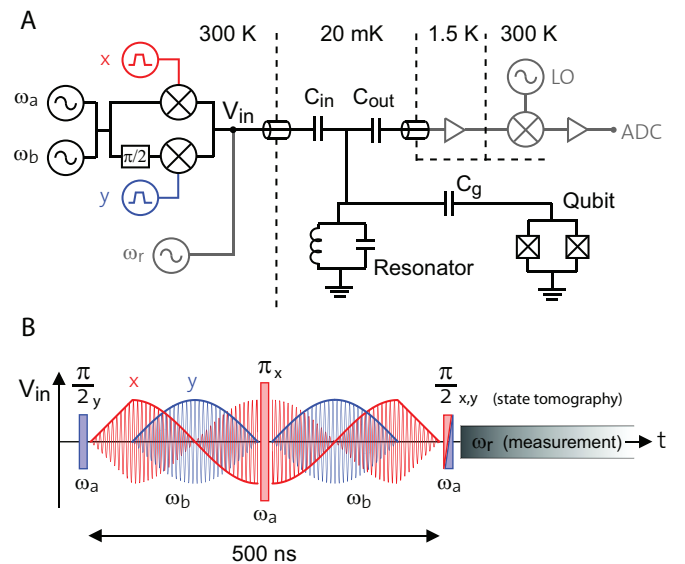

FIG. 2: (**A**) Simplified circuit diagram of the experimental setup. In the center at 20 mK is the resonator/qubit system, with the resonator represented by a parallel LC circuit, and the qubit, a split Cooper pair box, capacitively coupled to the resonator through C_{g}. The resonator is coupled to input and output transmission lines via the capacitors C_{in} and C_{out}. Three different pulse-modulated microwave frequency signals are applied to the resonator input. The two signals required for qubit manipulation, one at the qubit transition frequency $\omega_{\mathrm{a}}/2\pi$, and a detuned signal $\omega_{\mathrm{b}}/2\pi$ are modulated using mixers to the pattern shown in (B). The signal at the resonator frequency $\omega_{\mathrm{r}}/2\pi$, used to measure the qubit state, is turned on after the pulse sequence is applied. (**B**) Schematic pulse sequence for the case $n = 0.5$. Resonant pulses, shown as shaded rectangles, are 12 ns in length. The two quadrature bias microwave fields (x: red, y: blue) are represented as sinusoids with modulation amplitude shown by solid lines. The linear ramps at the start and end of these sections correspond to moving adiabatically between the $\Omega_{\mathrm{R}} = 0$ axis and the $\Omega_{\mathrm{R}} = $ const. circle (Fig. 1C).

in the opposite direction C_+, adds an additional phase $\phi_+ = \delta(t) + \gamma_C$. This results in total in a purely geometric phase $\phi = \phi_+ - \phi_- = 2\gamma_C$ being acquired during the complete sequence which we denote as C_{-+}. Note that unlike the geometric phase, the dynamic phase is insensitive to the path direction, and is hence completely canceled. At the end of the sequence, we extract the phase of the qubit state using quantum state tomography. In our measurement technique [26] the z component of the qubit Bloch vector $\langle \sigma_z \rangle$ is determined by measuring the excited state population $p_e = (\langle \sigma_z \rangle + 1)/2$. To extract the x and y components, a resonant $\pi/2$ pulse rotating the qubit about either the x or y axis is applied, and then the measurement is performed, revealing $\langle \sigma_y \rangle$ and $\langle \sigma_x \rangle$ respectively. The phase of the quantum state after application of the control sequence is then extracted as $\phi = \tan^{-1}(\langle \sigma_y \rangle / \langle \sigma_x \rangle)$.

In Fig. 3A we show the measured phase ϕ and its dependence on the solid angle of the path, for a number of different experiments, all carried out at $\Delta/2\pi \approx 50$ MHz, and total pulse sequence time $T = 500$ ns. Three parameters are varied; the path radius Ω_R (upper x-axis), the number of circular loops traversed in each half of the spin echo sequence, n, and the direction of traversal of the paths (C_{-+} and C_{+-}). The measured phase is in all cases seen to be linear in solid angle as Ω_R is swept, with a root-mean-squared deviation across all data sets of 0.14 rad from the expected lines of slope $2n$. Thus, all results are in close agreement with the predicted Berry's phase and it is clearly demonstrated that we are able to accurately control the amount of phase accumulated geometrically. Also we note that the dynamic phase is indeed effectively eliminated by the spin echo. Reversing the overall direction of the paths is observed to invert the sign of the phase (Fig. 3A). Traversing the circular paths on either side of the spin echo pulse in the same direction (C_{++}) as a control experiment is shown to result in zero measured phase (Fig. 3A).

To observe a pure Berry's phase, the rate of rotation of the bias field direction must be much less than the Larmor rate R of the qubit in the rotating frame, to ensure adiabatic qubit dynamics. For the case of constant cone angle θ, this translates to the requirement $A = \dot{\varphi}_R \sin\theta/2R \ll 1$. If the Hamiltonian is changed non-adiabatically, the qubit state can no longer exactly follow the effective field $\boldsymbol{R}$, and the geometric phase acquired deviates from Berry's phase [28]. For the experiments here, $A \leq 0.04$, and deviation of the measured phase from Berry's phase is not discernable. We have also verified experimentally that in this adiabatic limit the observed phase is independent of the total sequence time T.

In Fig. 3B, a measurement of the x and y components of the qubit state from which the Berry's phase is extracted is shown. Interestingly, the visibility of the observed interference pattern is seen to have a dependence
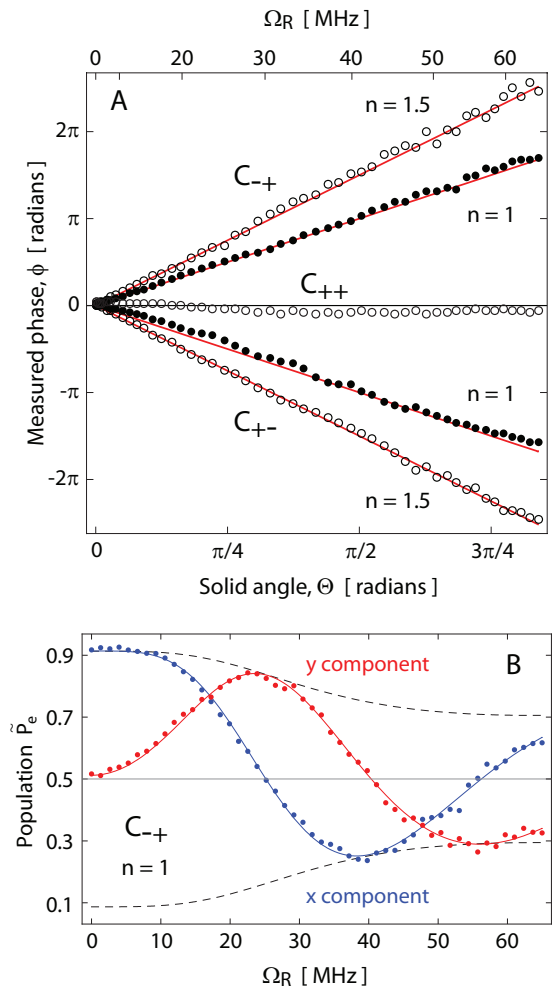

FIG. 3: (**A**) Measured phase ϕ versus solid angle Θ of a single conical path (lower axis). The applied microwave field amplitude is indicated on the upper axis (in units of the induced Rabi frequency Ω_R for resonant driving). Closed circles correspond to experiments in which $n = 1$ circular paths are traversed during each half of the spin echo sequence, and filled circles to the case $n = 1.5$. Subscripts $\pm$ of labels $C_{\pm\pm}$ correspond to the path direction before and after the spin echo π pulse. Red solid lines are of slope $n = \pm 1, \pm 1.5$. The C_{++} experiment was carried out with $n = 1.5$. (**B**) State tomography data for the C_{-+} experiment with $n = 1$. Plotted is the qubit excited state population after tomography pulses to extract $\langle \sigma_x \rangle$ (blue, $p_e = (\langle \sigma_x \rangle + 1)/2$) and $\langle \sigma_y \rangle$ (red, $p_e = (\langle \sigma_y \rangle + 1)/2$). Lines are fits to Berry's phase, with a geometric dephasing envelope function (dashed lines, described in the text and Fig. 4). In all cases, the total pulse sequence time is $T = 500$ ns, and the detuning is $\Delta/2\pi \approx 50$ MHz. To accumulate measurement statistics sequences are repeated 2×10^5 times.

on Ω_R. Since the data is taken at fixed total sequence time, this is not due to conventional T_2 dephasing, which is also independently observable as a function of time, but can be explained as due to geometric dephasing, an effect dependent on the geometry of the path [29].
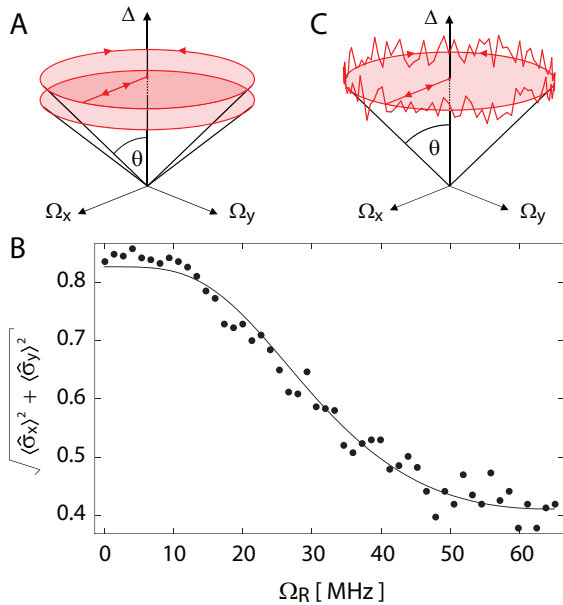
FIG. 4: (**A**) Low frequency fluctuations in Δ change the solid angle enclosed by the path from one measurement to the next, and cause geometric dephasing with a characteristic dependence on the cone angle and bias field amplitude. (**B**) Magnitude of the equatorial component of the Bloch vector $(\langle\sigma_{\rm x}\rangle^2 + \langle\sigma_{\rm y}\rangle^2)^{1/2}$ for the data shown in Fig. 3B, plotted as a function of drive amplitude $\Omega_{\rm R}$. The fit is to a geometric dephasing factor $e^{-\sigma_\gamma^2/2}$ where σ_γ^2 is the variance of the geometric phase. (**C**) The conical parameter space path in the presence of high frequency ($f \gg T^{-1}$) noise in Δ, having no effect on the total solid angle.

In our experiment, dephasing is dominated by low frequency fluctuations in the qubit transition frequency $\omega_{\rm a}$ (and thus Δ) induced by charge noise coupling to the qubit [30]. The spin echo pulse sequence effectively cancels the dynamic dephasing due to the low frequency noise. However, the geometric phase is sensitive to slow fluctuations, since they cause the solid angle subtended by the path at the origin to change from one measurement to the next (see Fig. 4A). The effect on the geometric phase of such fluctuations in the classical control parameters of the system has been studied theoretically [29]. In the limit of the fluctuations being slower than the time scale of the spin echo sequence, the variance of the geometric phase σ_γ^2 has itself a purely geometric dependence, $\sigma_\gamma^2 = \sigma_\omega^2(2n\pi \sin^2\theta/R)^2$, where σ_ω^2 is the variance of the fluctuations in $\omega_{\rm a}$ [29]. In Fig. 4B, we show the observed dependence of the coherence on geometry explicitly by plotting $(\langle\sigma_{\rm x}\rangle^2 + \langle\sigma_{\rm y}\rangle^2)^{1/2}$ versus $\Omega_{\rm R}$, which fits well to the expected dependence $e^{-\sigma_\gamma^2/2}$. This is also in agreement with the raw data in Fig. 3B.

Hence we have observed an important geometric contribution to dephasing that occurs when geometric operations are carried out in the presence of low frequency fluctuations. In contrast, higher frequency noise in $\omega_{\rm a}$ is expected to have little influence on Berry's phase (provided adiabaticity is maintained), since its effect on the solid angle is averaged out (see Fig. 4C). This characteristic robustness of geometric phases to high frequency noise may be exploitable in the realization of logic gates for quantum computation, although the effect of geometric dephasing due to low frequency noise must be taken into account.

[1] A. Shapere, F. Wilczek, *Geometric Phases in Physics* (World Scientific, Singapore, 1989).
[2] J. Anandan, *Nature* **360**, 307 (1992).
[3] M. V. Berry, *Proc. R. Soc. London Ser. A* **392**, 45 (1984).
[4] M. A. Nielsen, I. L. Chuang, *Quantum Computing and Quantum Information* (Cambridge University Press, 2000).
[5] J. A. Jones, V. Vedral, A. Ekert, G. Castagnoli, *Nature* **403**, 869 (2000).
[6] D. Leibfried *et al.*, *Nature* **422**, 412 (2003).
[7] G. Wendin, V. Shumeiko, *Handbook of Theoretical and Computational Nanotechnology*, M. Rieth, W. Schommers, eds. (American Scientific Publishers, 2006), vol. 3 (*arXiv:cond-mat/0508729v1*).
[8] M. H. Devoret, A. Wallraff, J. M. Martinis, *arXiv:cond-mat/0411174v1* (2004).
[9] T. Yamamoto, Y. A. Pashkin, O. Astafiev, Y. Nakamura, J. S. Tsai, *Nature* **425**, 941 (2003).
[10] M. Steffen *et al.*, *Science* **313**, 1423 (2006).
[11] A. O. Niskanen *et al.*, *Science* **316**, 723 (2007).
[12] J. H. Plantenberg, P. C. de Groot, C. J. P. M. Harmans, J. E. Mooij, *Nature* **447**, 836 (2007).
[13] J. Majer *et al.*, *Nature* **449**, 443 (2007).
[14] M. A. Sillanpää, J. I. Park, R. W. Simmonds, *Nature* **449**, 438 (2007).
[15] G. Falci, R. Fazio, G. M. Palma, J. Siewert, V. Vedral, *Nature* **407**, 355 (2000).
[16] X. B. Wang, M. Keiji, *Phys. Rev. B* **65**, 172508 (2002).
[17] A. Blais, A. M. S. Tremblay, *Phys. Rev. A* **67**, 012308 (2003).
[18] Z. H. Peng, M. J. Zhang, D. N. Zheng, *Phys. Rev. B* **73**, 020502 (2006).
[19] M. Mottonen, J. P. Pekola, J. J. Vartiainen, V. Brosco, F. W. J. Hekking, *Phys. Rev. B* **73**, 214523 (2006).
[20] Y. Nakamura, Y. A. Pashkin, J. S. Tsai, *Nature* **398**, 786

(1999).

[21] A. Shnirman, G. Schön, Z. Hermon, *Phys. Rev. Lett.* **79**, 2371 (1997).

[22] V. Bouchiat, D. Vion, P. Joyez, D. Esteve, M. H. Devoret, *Phys. Scr.* **T76**, 165 (1998).

[23] D. Vion *et al.*, *Science* **296**, 886 (2002).

[24] A. Blais, R. S. Huang, A. Wallraff, S. M. Girvin, R. J. Schoelkopf, *Phys. Rev. A* **69**, 062320 (2004).

[25] A. Wallraff *et al.*, *Nature* **431**, 162 (2004).

[26] A. Wallraff *et al.*, *Phys. Rev. Lett.* **95**, 060501 (2005).

[27] A. Abragam, *Principles of Nuclear Magnetism* (Oxford University Press, 1961).

[28] Y. Aharonov, J. Anandan, *Phys. Rev. Lett.* **58**, 1593 (1987).

[29] G. De Chiara, G. M. Palma, *Phys. Rev. Lett.* **91**, 090404 (2003).

[30] G. Ithier *et al.*, *Phys. Rev. B* **72**, 134519 (2005).